CRYSTAL GROWTH & DESIGN

Article

pubs.acs.org/crystal

Lornoxicam Salts: Crystal Structures, Conformations, and Solubility

Kuthuru Suresh and Ashwini Nangia*

School of Chemistry, University of Hyderabad, Prof. C. R. Rao Road, Gachibowli, Central University P.O., Hyderabad 500 046, India

Supporting Information

ABSTRACT: Lornoxicam (LXM), a nonsteroidal anti-inflammatory drug (NSAID), is an amphiprotic molecule that exists as a zwitterion in the solid state. The formation of two strong intramolecular $N^+-H\cdots O$ and $N-H\cdots O^-$ hydrogen bonds in a stable six-member ring geometry, $S(6)$, renders this otherwise flexible molecule in a rigid conformation (conformer A). A salt screen of LXM was undertaken to improve drug solubility and to study different conformations of the molecule by varying the counterion. As an amphoteric molecule, LXM salts are both cationic (ammonia, piperazine) and anionic (hydrochloric acid, methanesulfonic acid). The crystal structures of these salts exhibit an intramolecular H bond with different conformations of LXM in the acid and base salts (conformations B and C). The conformational variability of LXM in acidic and basic salts is explained by steric and hydrogen bonding factors. All the new salts were characterized by spectroscopic, thermal, powder X-ray diffraction techniques and showed enhanced solubility compared to the free drug.

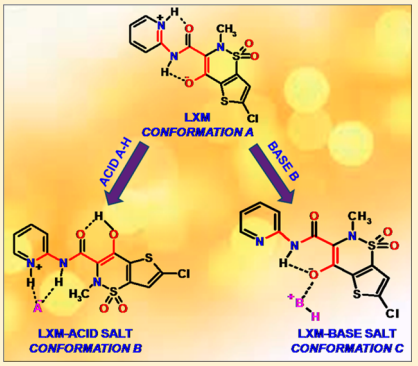

Downloaded via UNIV OF PITTSBURGH on January 23, 2026 at 20:40:53 (UTC).
See https://pubs.acs.org/sharingguidelines for options on how to legitimately share published articles.

INTRODUCTION

Salt formation is the first line method for improving the physicochemical properties of active pharmaceutical ingredients (APIs), such as dissolution rate, bioavailability, and stability.[1] The modification of an acidic or a basic API as a salt form gives higher solubility and stability together with improved flowability, filterability, etc. The conversion of an acidic or basic or amphoteric API to a salt can also change its biological properties and offer novel patentable forms.[2] Pharmaceutical salts[1] are the most important solid-state modifications that are formed between an ionic API and suitable, pharmaceutically acceptable Generally Recognized As Safe (GRAS)[3] coformers as counterions. They have been an integral part of the crystal form screen and selection process in the pharmaceutical industry. Other solid-state forms such as polymorphs,[4] cocrystals,[5] amorphous phases along with several other methods for solubility enhancement, e.g., eutectics,[6] solid dispersions,[7] and amorphous phases,[8] are known in the prior art. The pharmaceutical salt strategy to improve the solubility and dissolution rate of BCS class II drugs (Biopharmaceutics Classification System)[9] having ionizable functional groups[10] is discussed for lornoxicam in this paper.

Lornoxicam[11] (LXM hereafter; Scheme 1) is a nonsteroidal anti-inflammatory drug (NSAID) with analgesic, anti-inflammatory, and antipyretic properties. It is marketed under the brand names Lorcam and Xafon.[12] LXM is an oxicam class drug in the BCS II category with low solubility and high permeability (solubility of LXM in water 15 mg/L).[13] Cyclodextrin complexes[14a] and solid dispersions[14b] are reported to improve the solubility and bioavailability of LXM. Polymorphs and cocrystals of LXM have been reported and characterized by using powder X-ray diffraction.[13,15] We explored LXM salts to study the effect of counterions on solubility, stability, and conformation in the crystal structure.

RESULTS AND DISCUSSION

We obtained crystalline salts of LXM with hydrochloric acid (HCl), methanesulfonic acid (MSA), piperazine (PIP), and ammonia (AMM). LXM adopts three conformations (designated as A, B, and C) in crystal structures (see Scheme 1). LXM is an amphiprotic molecule containing a β-keto–enol group on chlorothianothiazine ring, which is connected to a pyridyl ring through the imide group (Scheme 1). In the guest-free structure, the molecule adopts conformer A because of internal proton transfer and intramolecular hydrogen bond, which lock the molecular flexibility (Figure 1; see ORTEP in Figure S1a, Supporting Information). The guest-free LXM exists as a zwitterion with proton transfer from the β-keto–enolic OH group to the pyridine N, but there is no hydrogen bonding between them as the groups are far apart (Figure 1). The competing N–H acceptor of the imide group cannot abstract the proton, though its pK_a is higher than the pyridine N (Table 1), because of the electron-withdrawing effect of the flanking C=O (of imide) and pyridyl groups.[16,17] It forms an intramolecular hydrogen bond with the β-keto–enolate group ($N-H\cdots O^-$, 2.61 Å, 140°), which also eliminates repulsion between the adjacent imide NH, pyridyl NH^+, imide C=O, and enolic C–O groups. These repelling groups point away from each other in conformation A, with an intramolecular H bond $N^+-H\cdots O$ (2.54 Å, 134°) (Figure 1). Two intramolecular hydrogen bonds in the energetically favorable six-membered

Received: February 14, 2014
Revised: April 24, 2014
Published: April 25, 2014

 © 2014 American Chemical Society dx.doi.org/10.1021/cg500231z | *Cryst. Growth Des.* 2014, 14, 2945–2953

Ascletis Ex. 2075
Page 1 of 9

Scheme 1. (a) LXM and Salt Formers Used in This Study and (b) Different Conformations of LXM in Salt Structures

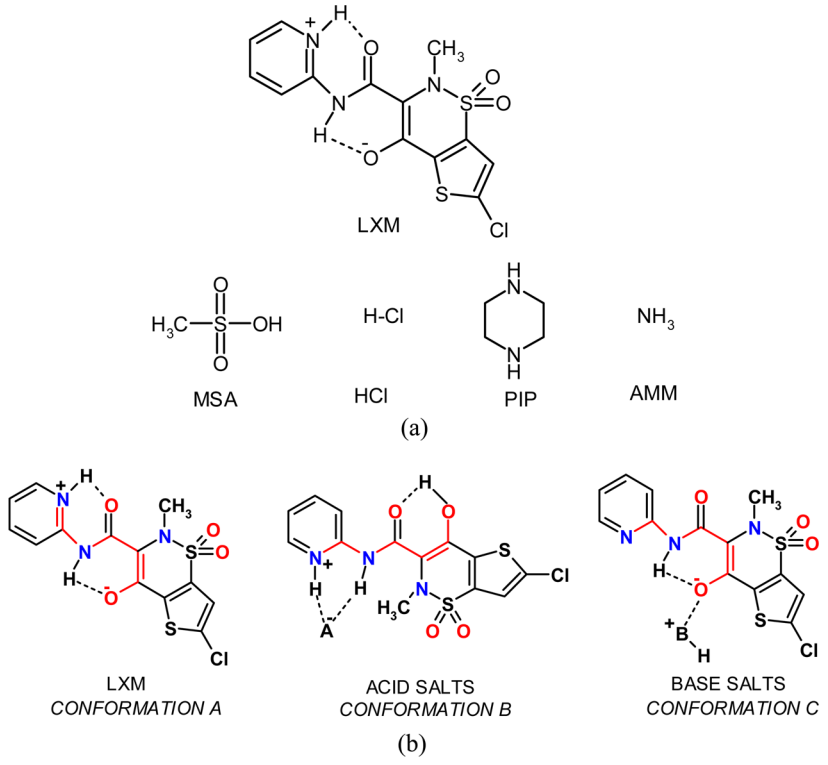

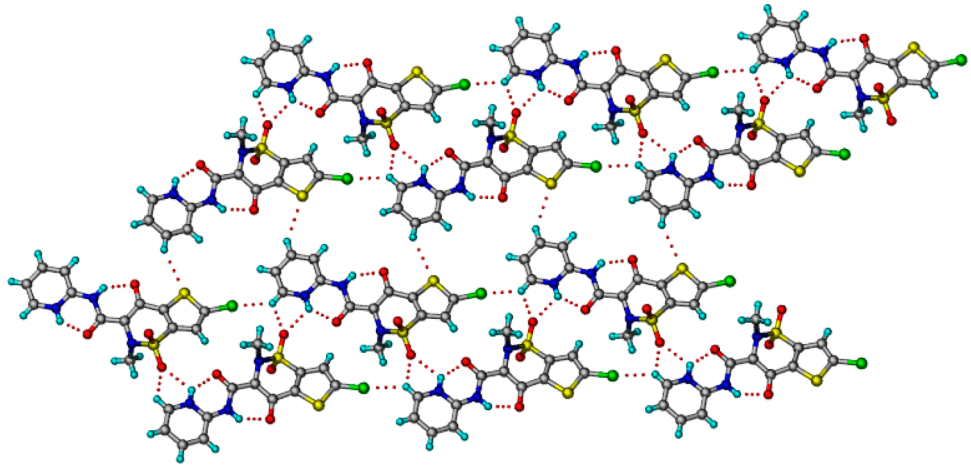

Figure 1. Layered section of lornoxicam molecules connected via N^+–H···O, N–H···O^- H bonds and weaker C–H···Cl, C–H···O, C–H···S interactions.

Table 1. Coformers Resulting in Salts with Lornoxicam and Their ΔpK_a Values[a]

	pK_a in water	ΔpK_a	molecular structure
LXM	1.82, 4.22	2.40	zwitterionic
HCl	−7.00	11.22	1:1 salt
MSA	−1.61	5.83	1:1 salt
PIP	9.72	7.90	1:0.5 salt
AMM	8.86	7.04	1:1 salt

[a] pK_a's were calculated using Marvin 5.10.1, 2012, ChemAxon (http://www.chemaxon.com).[20]

ring geometry ($S(6)$ graph set pattern)[18] and linear tapes of such LXM molecules extend in a sheet structure.

Given the solubility advantage of salts, and the importance of structural and conformational control,[10,19] which can be influenced by strong hydrogen bonding and counterions, we explored a salt screen of LXM with two strong acids (HCl and MSA) and two strong bases (PIP and AMM). The high ΔpK_a's (Table 1) will result in salts.

Crystal Structures of LXM Salts. The crystal structures of HCl and MSA salts show that the β-keto–enolic proton is intact on the LXM molecule but the pyridyl group is protonated (Figures 2 and 3; see ORTEP in Figure S1b,c, Supporting Information). The strong acids donate proton to the pyridyl group compared to the weaker β-keto–enol moiety. Understandably the imide NH cannot be protonated because of electronic and steric effects. In this situation, the H–H repulsion between imide N–H and β-keto–enolic proton and

dx.doi.org/10.1021/cg500231z | Cryst. Growth Des. 2014, 14, 2945–2953
Ascletis Ex. 2075
Page 2 of 9

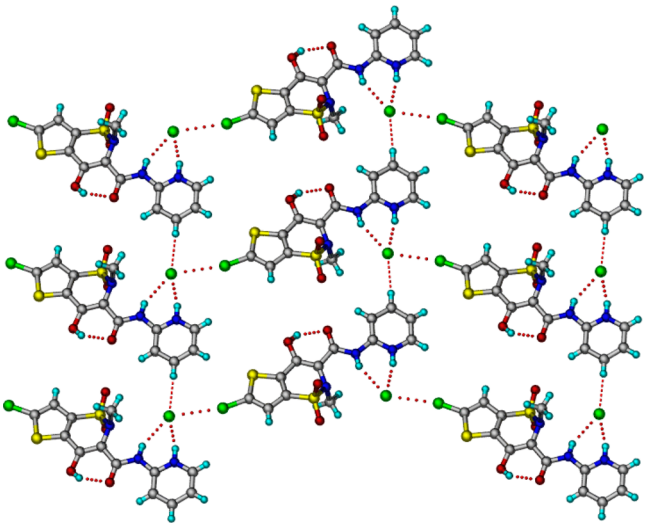

Figure 2. Linear tapes are connected via C−H···Cl^- interactions between the R_2^1 (6) ring motifs of pyridinium NH^+ and imide NH with a chloride ion and extend through Cl···Cl^- interactions in the structure of LXM−HCl salt.

the energetic advantage of intramolecular $S(6)$ H-bond in the β-keto−enol group (Figure 2) invoke a conformational change in LXM molecule. In effect, the imide bond rotates such that imide keto group makes an intramolecular hydrogen bond with un-ionized β-keto−enol through O3−H3A···O4 (2.52 Å, 135°) with the $S(6)$ O···H···O ring motif and imide NH makes a hydrogen bond with the anion (chloride or mesylate). Both the intramolecular N/N^+−H··· O^-/O bonds of conformer A in the guest-free structure of LXM are replaced by a new intramolecular β-keto−enol O···H···O hydrogen bond in the acid salts. The imide NH and pyridyl NH^+, and imide C═O and enolic OH groups become syn-oriented to each other (trans-orientation in conformer A), and form a new conformation B which is same in both salts (Figure 2 and 3; see ORTEP in Figure S1b,c, Supporting Information).

Lornoxicam hydrochloride salt (1:1) structure was solved in the orthorhombic space group $P2_12_12_1$. The syn-oriented pyridinium NH^+ and imide NH form intermolecular H bonds with a chloride ion ($N1^+$−H1···Cl^- 2.14 Å, 166°; N2−H2A···Cl^- 2.45 Å, 148°) in a R_2^1 (6) motif. Such units are connected as linear tapes via C−H···Cl^- interactions which further extend in a layer through Cl···Cl^- interactions.

Lornoxicam mesylate salt (1:1) solved in the monoclinic space group $P2_1/c$. The syn-oriented pyridinium NH^+ and imide NH form intermolecular hydrogen bonds with a sulfonate ion ($N1^+$−H1···$O6^-$ 1.83 Å, 109°; N2−H2A···O7 2.03 Å, 121°) in a $R_2^2(8)$ motif, which are connected via $Cl_{(LXM)}$···$O_{(MSA)}$ interaction (C12−Cl22···O6 3.12 Å, 109°), which propagate as antiparallel tapes through the β-keto−enol sulfonyl H bond (O3−H3A···O2−S1 2.21 Å, 130°) interactions. Crystal data are summarized in Table 2, and hydrogen bonds are listed in Table 3.

The crystal structures of PIP and AMM salts show that the β-keto−enol proton of LXM is transferred to the added base (Figures 4 and 5; see ORTEP in Figure S1d,e) in competition to the internal pyridyl group which is weaker (see pK_a values in Table 1). As a result, the pyridyl group remains un-ionized; the intramolecular H-bond with the imide keto group of conformer A is absent. Moreover, the repulsion between the pyridine N and imide O atoms results in rotation of the pyridyl ring such that it forms a hydrogen bond with the NH^+ of piperazine or ammonium ion donor (Figure 4 and 5). This new LXM conformation C has a syn-oriented imide NH and pyridyl N (as in the acid salts) and trans-oriented imide C═O and enol C−O^-, whereas the imide NH and enolate are involved in intramolecular hydrogen bonding. The effect of the counterions on the conformational changes of LXM is depicted in Scheme 2.

Lornoxicam ammonium salt (1:1) crystallized in $P\bar{1}$ space group. The ammonium ion forms intermolecular ionic hydrogen bonds with enolate anion ($N4^+$−H4A···$O3^-$ 2.19 Å, 143°; $N4^+$−H4B···$O3^-$ 1.83 Å, 174°) and pyridine ($N4^+$−H4D···N1 2.05 Å, 158°) in a $R_4^2(8)$ motif. Such motifs are bonded via $R_3^2(8)$ ring motifs about the inversion center and extend through ammonium cation−sulfonyl interactions.

Lornoxicam piperazinium salt crystallized as a 1:0.5 salt consistent with the acid−base donor−acceptor ratio. One LXM and half PIP are present in the asymmetric unit of a monoclinic $P2_1/c$ crystal structure. The PIP dication lies about an inversion

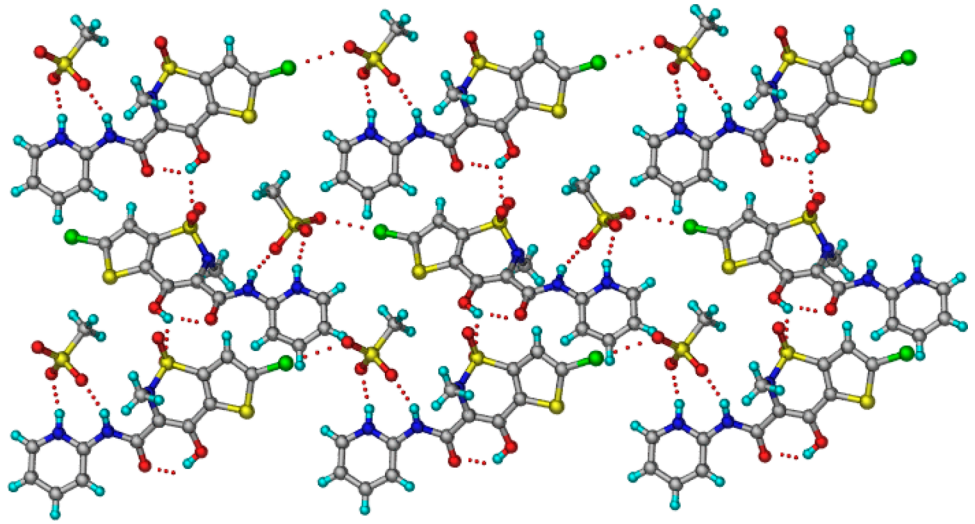

Figure 3. Linear tapes are formed by Cl···O interaction between the R_2^2 (8) motifs of pyridinium NH^+ and imide NH with mesylate ion propagate as antiparallel tapes through H bonding with the β-keto−enol sulfonyl moiety.

dx.doi.org/10.1021/cg500231z | Cryst. Growth Des. 2014, 14, 2945−2953

Ascletis Ex. 2075
Page 3 of 9

Table 2. Crystallographic Parameters of LXM Salts

	LXM	LXM−HCl	LXM−MSA	LXM−PIP	LXM−AMM
emp form.	$C_{13}H_{10}N_3O_4S_2Cl$	$C_{13}H_{11}N_3O_4S_2Cl_2$	$C_{14}H_{14}N_3O_7S_3Cl$	$C_{15}H_{16}N_4O_4S_2Cl$	$C_{13}H_{13}N_4O_4S_2Cl$
form. wt	371.81	408.29	467.94	414.90	388.86
cryst syst	orthorhombic	orthorhombic	monoclinic	monoclinic	triclinic
sp gr	$P2_12_12_1$	$P2_12_12_1$	$P2_{1/c}$	$P2_{1/c}$	$P\bar{1}$
T (K)	298(2)	298(2)	298(2)	298(2)	298(2)
a (Å)	7.2020(4)	6.8795(5)	13.4730(11)	13.2445(9)	7.5577(7)
b (Å)	13.5420(8)	9.1606(8)	13.2684(8)	13.0698(7)	10.3747(9)
c (Å)	14.9987(7)	26.201(2)	11.2407(8)	11.6414(8)	12.0879(12)
α (deg)	90	90	90	90	68.516(9)
β (deg)	90	90	111.707(9)	111.547(8)	75.433(8)
γ (deg)	90	90	90	90	70.585(8)
Z	4	4	4	4	2
V (Å^3)	1462.82(14)	1651.2(2)	1867.0(3)	1874.3(2)	822.65(15)
rflns collect	4334	4783	8057	7900	5347
unique rflns	2731	3204	3818	3832	3353
obsd rflns	1976	1699	2030	2377	1908
parameters	209	219	256	236	269
R_1	0.0483	0.0707	0.0507	0.0406	0.0692
wR_2	0.1031	0.1586	0.0828	0.0984	0.1513
GOF	0.960	0.980	0.907	0.905	0.972
diffractometer	Oxford Xcalibur Gemini	Oxford Xcalibur Gemini	Oxford Xcalibur Gemini	Oxford Xcalibur Gemini	Oxford Xcalibur Gemini

center (protons abstracted each from two lornoxicam molecules) and bridges the molecules through N^+−H···O^- hydrogen bonds (1.75 Å, 167°). Additional C−H···N interaction between the CHs of piperazinium ion and LXM pyridine together with heteroatom O···Cl interactions strengthen the structure.

Characterization of Salts. *PXRD.* Powder X-ray diffraction[21] enables a rapid identification of new crystalline salts. PXRD of experimental and calculated (obtained from the X-ray crystal structure) patterns of the salts showed excellent superposition to confirm phase purity of the bulk samples (Figure 6).

IR. Infrared spectroscopy[22] provides information about vibrational modes in a molecule due to changes in molecular conformations and hydrogen bonding. LXM exhibits the amide carbonyl stretch at 1646 cm^{-1}, the enolate peak at 1623 cm^{-1}, and the pyridine N^+−H stretch broad peak at 3444 cm^{-1}. These functional groups showed significant changes in their vibrational patterns on salt formation. In LXM−HCl and LXM−MSA the amide carbonyl stretching frequency is blue-shifted to 1657 and 1666 cm^{-1}. The β-keto−enol frequency resonates at 1633 and 1631 cm^{-1}, and pyridine N^+−H at 3447 and 3441 cm^{-1} (broad). In LXM−PIP and LXM−AMM the β-keto−enolate peak is at 1625 and 1612.7 cm^{-1}. PIP and AMM salts N^+−H broad stretching vibration peak at 3414 and 3438.1 cm^{-1}. FT-IR spectra are displayed in Figure S2, Supporting Information.

ss-NMR. Solid state NMR spectroscopy[23] is informative about short-range order in the solid-state and complements PXRD. We analyzed of all the compounds, and we observed interesting changes in LXM salts ^{13}C ss-NMR spectra. The LXM enol group which is deprotonated in the guest-free form and the base salts showed similar chemical shift values (δ LXM 107.8, LXM−PIP 111.47, LXM−AMM 109.13; Figure 7 and Table S1, Supporting Information), thus indicating that the chemical environment around the enolate group is similar in these structures (see Scheme 2 for conformers A and C which have a trans-oriented enol C−O^- and imide C═O groups). In acid salts, the LXM enol proton makes an intramolecular H bond (conformer B, δ ∼190 ppm) compared to enolic C−O^- of guest-free LXM and base salts ($\delta \approx$ 109 ppm). The ss-NMR spectra not only characterized the salts but also correlated with the NMR peaks positions.

Thermal Analysis. Differential scanning calorimetry (DSC)[24] is characteristic in establishing the purity of the component and phase changes upon heating. An exotherm peak in LXM at 210 °C (decomposition) as well as its salts (at slightly different temperatures) indicating decomposition of the drug.[17b] LXM−HCl and LXM−AMM exhibited a weak endotherm followed by the major exotherm peak (Figure S3, Table 4).

Solubility and Powder Dissolution. The bioavailability and efficacy of a drug largely depend upon its solubility and dissolution rate in the aqueous medium. Solubility and permeability of a drug molecule determine its mode of administration into the body. Altering the physicochemical properties of a drug can change bioavailability[25] and therapeutic action. Solubility and powder dissolution of the new salts was performed in pH 7 phosphate buffer (neutral) medium. Solubility of LXM−HCl and LXM−MSA salts could not be determined as they dissociated to the parent LXM within 24 h. The stable LXM−PIP and LXM−AMM salts exhibited 7.0 and 2.3 times higher solubility than the parent drug. PXRD plots of the undissolved residue at the end of the equilibrium solubility experiment (Figure S4, Supporting Information) confirm that there is no phase transformation[26] or degradation of the base salts during the solubility experiment. Dissolution is a time-dependent phenomenon which can estimate the apparent solubility of compounds and hence this method is preferable for solids which undergo phase transformation during the solubility measurements (see stability PXRD in Figure S5, Supporting Information). Powder dissolution was carried out on all compounds and the PDRs at 60 min of peak solubility are LXM−MSA 158 mg/L > LXM−HCl 143 mg/L > LXM−AMM 133 mg/L > LXM−PIP 127 mg/L > LXM 100 mg/L. The equilibrium solubility of LXM and its base salts LXM−PIP

dx.doi.org/10.1021/cg500231z | Cryst. Growth Des. 2014, 14, 2945−2953
Ascletis Ex. 2075
Page 4 of 9

Table 3. Hydrogen Bonds in LXM Salts[a]

D−H···A	D···A (Å)	H···A (Å)	D−H···A (deg)	symmetry code
		LXM		
N1−H1···O4	2.545(4)	1.87	134	*b*
N1−H1···O1	3.008(5)	2.45	124	1/2−*x*,1−*y*, −1/2+*z*
N2−H2A···O3	2.611(4)	1.89	140	*b*
C2−H2···O2	3.295(5)	2.51	142	1−*x*,−1/2+*y*,1/2−*z*
C4−H4···O2	3.332(4)	2.39	123	−1/2+*x*,1/2−*y*, −*z*
C5−H5···Cl	3.407(3)	2.67	137	*x*, *y*, −1+*z*
C11−H11···O4	3.227(5)	2.32	165	1/2−*x*,1−*y*, −1/2+*z*
		LXM−HCl		
N1−H1···Cl2	2.976(7)	2.13	166	−1/2+*x*,1/2−*y*, −*z*
N2−H2A···Cl2	3.217(6)	2.46	148	*x*, *y*, *z*
N2−H2A···N3	2.785(8)	2.39	108	*b*
O3−H3A···O4	2.528(7)	1.88	135	*b*
C3−H3···Cl2	3.530(8)	2.60	177	*x*,1+*y*,*z*
C5−H5···O1	3.265(10)	2.38	160	−1/2+*x*,1/2−*y*, −*z*
		LXM−MSA		
N1−H1···O5	2.673(4)	1.83	167	*x*, *y*, *z*
N2−H2A···O7	2.845(4)	2.03	157	*x*, *y*, *z*
N2−H2A···N3	2.727(3)	2.32	109	*b*
O3−H3A ···O4	2.638(3)	1.95	142	*b*
O3 −H3A···O2	2.819(4)	2.21	131	−*x*, −1/2+*y*,1/2−*z*
C14−H14C···O6	3.384(5)	2.45	165	1−*x*,1−*y*,1−*z*
		LXM−PIP		
N2−H2A···O3	2.649(2)	1.92	142	*b*
N4−H4A···O3	2.642(3)	1.76	168	*x*,1/2−*y*, −1/2+*z*
N4−H4B···O4	2.730(2)	1.90	151	*x*,1/2−*y*, −1/2+*z*
C2−H2···O4	2.914(3)	2.34	120	*b*
C15−H15A···O4	3.215(3)	2.53	128	1−*x*, −1/2+*y*,1/2−*z*
		LXM−AMM		
N2−H2A···O3	2.702(5)	2.06	144	*b*
N4−H4A···O1	3.020(6)	2.51	118	−1+*x*,*y*,*z*
N4−H4A···O3	2.945(7)	2.19	143	1−*x*, −*y*,1−*z*
N4−H4B···O3	2.835(6)	1.83	174	−*x*, −*y*,1−*z*
N4−H4C···O4	2.849(6)	1.99	162	−1+*x*,*y*,*z*
N4−H4D···N1	2.956(7)	2.05	158	*x*, *y*, *z*
C2−H2···O4	3.218(6)	2.58	133	2−*x*,1−*y*,1−*z*
C11−H11···O2	3.285(6)	2.37	155	3−*x*, −*y*, −*z*
C1−H13C···O4	3.213(7)	2.58	128	*b*

[a]N−H, O−H, and C−H distances were neutron-normalized. [b]Intramolecular hydrogen bond.

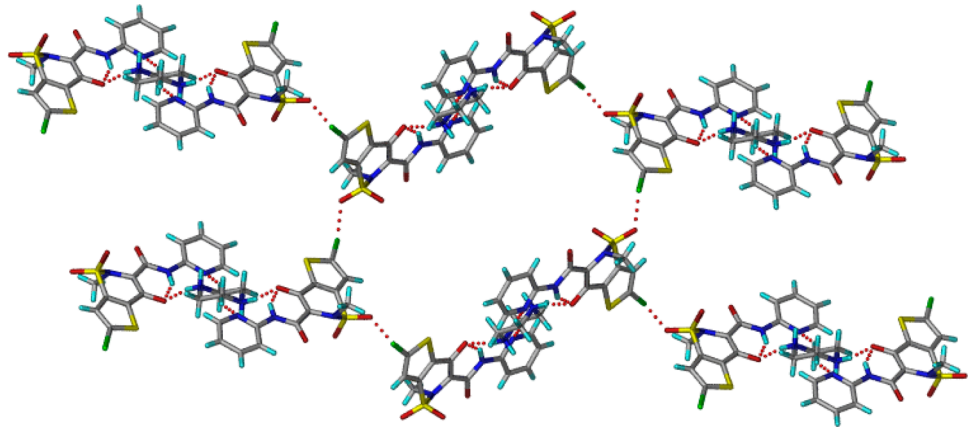

Figure 4. LXM−PIP molecules are connected through N^+−H···O^- and C−H···N interactions and form an inversion center, and linear tapes are formed by O···Cl interactions. ID tapes are propagate as antiparallel tapes in 2D via through O···Cl interactions.

are 2355 mg/L > LXM−AMM 879 mg/L > LXM 339 mg/L. In summary, the acid salts have a higher apparent solubility/PDR than the basic salts, and overall the salts are superior to the reference drug (Figure 8, dissolution rates and $AUC_{0-60\ min}$ are

dx.doi.org/10.1021/cg500231z | *Cryst. Growth Des.* 2014, 14, 2945−2953
Ascletis Ex. 2075
Page 5 of 9

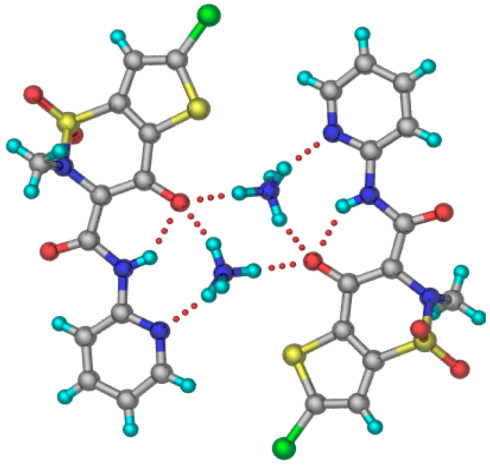

Figure 5. N−H···O hydrogen bond ring motifs in the crystal structure of LXM−AMM salt.

Scheme 2. Different Conformations of LXM

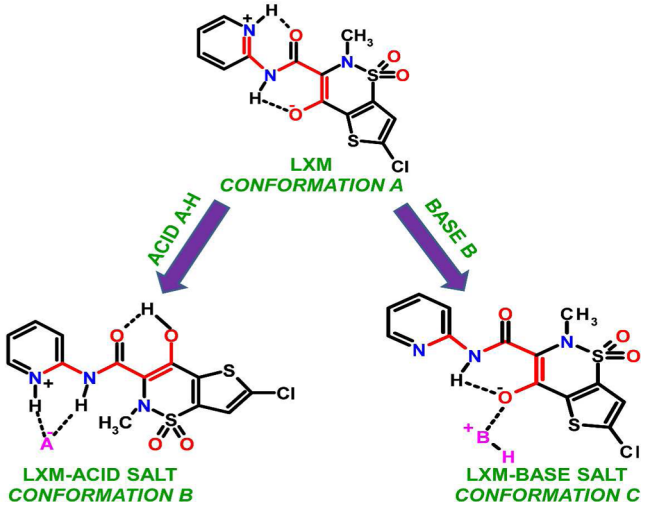

listed in Table 5). LXM and its basic salts did not show any form conversion, but the acidic salts converted to LXM after 90 min.

CONCLUSIONS

A salt screen of LXM gave a better understanding of the effect of counterion on conformational changes in the drug molecule. Strong acids and bases changed the conformational flexibility by changes in intramolecular hydrogen bonding LXM to give conformations A, B, and C. All the new salts exhibited good solubility and powder dissolution rate than the parent drug LXM. LXM salts with acids exhibited higher solubility than the base salts, e.g., LXM−MSA salt has two times higher AUC compared to PIP and AMM salts. However, the base salts are more stable than the acid salts, in line with the solubility−stability inverse correlation. This is a systematic study of conformational changes in a drug molecule due to counterion and partner molecules. The present study with LXM salts offers acidic and basic counterions for an amphoteric drug to improve its physicochemical properties.

EXPERIMENTAL SECTION

Lornoxicam was purchased from Mesochem Import & Export Co. Ltd., China. Solvents (purity > 99%) and other coformers were

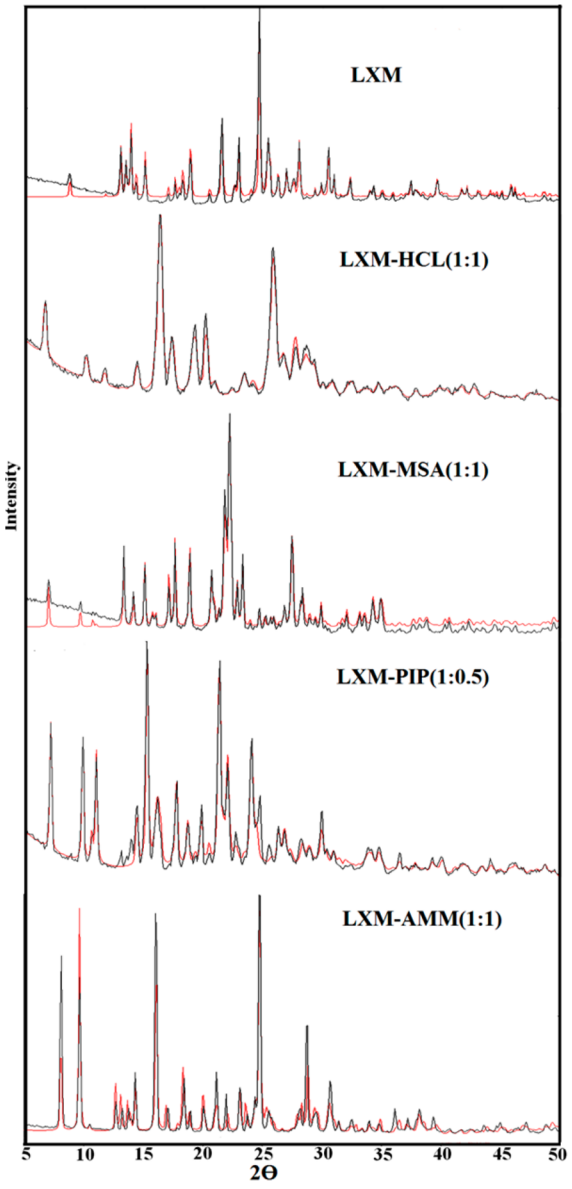

Figure 6. Overlay of experimental PXRD patterns of novel solid forms (black) showed a good match with their calculated line profile from the X-ray crystal structure (red) indicating bulk purity and phase homogeneity.

purchased from Hychem Laboratories (Hyderabad, India) and Sigma-Aldrich (Hyderabad, India). Water filtered through a double deionizer purification system (Aqua DM, Bhanu, Hyderabad, India) was used for all experiments.

Preparation of LXM Salts. *LXM−HCl.* To a solution of 250 mg of LXM in ethanol (5 mL), 2 mL of conc. HCl (37%) solution was added, and the slurry was ground for up to 45 min. The solution was filtered through Whatman filter paper, and salt formation (93% recovery) was confirmed by PXRD. A total of 40 mg of the salt was dissolved in nitromethane (5 mL) and left for slow evaporation at room temperature. Single crystals were obtained after 4 days.

LXM−MSA. A total of 372 mg of LXM and 96 mg of MSA (1:1 molar ratio) were dissolved in 5 mL of ethanol, and the slurry was ground for 1 h. The solid was filtered and confirmed as the salt (96%) by PXRD. A total of 40 mg of the salt was dissolved in EtOH−CH_3CN (3 mL + 2 mL) solvent mixture and left for slow evaporation at room temperature. Single crystals were obtained after 4 days.

LXM−PIP. A total of 372 mg of LXM and 43 mg of PIP (1:0.5 molar ratios) were dissolved in 5 mL of ethanol, and the slurry was ground

dx.doi.org/10.1021/cg500231z | *Cryst. Growth Des.* 2014, 14, 2945−2953

Ascletis Ex. 2075
Page 6 of 9

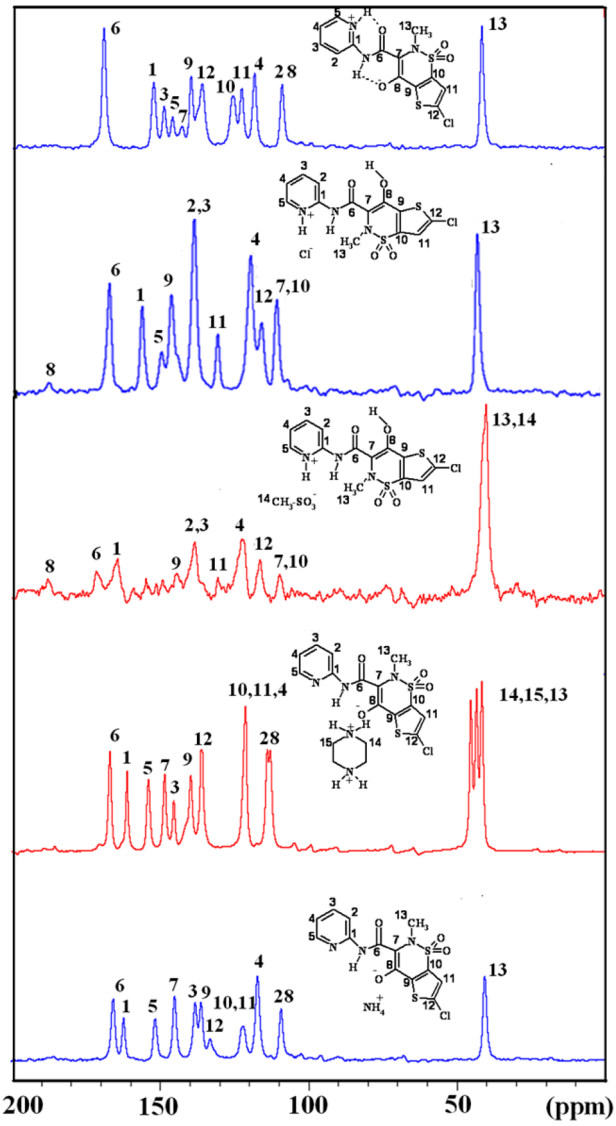

Figure 7. ss-NMR spectra of LXM and its salts (δ, ppm).

Table 4. Melting Point and Decomposition Temperature of LXM Salts from DSC[a]

s. no.	sample name	melting point of salt (°C)	decomposition of salt (°C)
1	LXM	*b*	210
2	LXM−HCl	175	221
3	LXM−MSA	*b*	205
4	LXM−PIP	*b*	193
5	LXM−AMM	165	221

[a]See Figure S2. [b]No endotherm observed.

for 1 h. The solid was filtered (95% recovery) and the material was confirmed as the salt by PXRD. A total of 40 mg of this salt was dissolved in nitromethane (5 mL) and left for slow evaporation at room temperature to harvest single crystals after 5 days.

LXM−AMM. To a solution of 250 mg of LXM in ethanol, 2 mL of conc. aqueous ammonia solution (25% conc.) was added, and the slurry was ground for 45 min. The solution was filtered through Whatman filter paper and salt product (92%) formation was confirmed by PXRD. A total of 40 mg of the salt was dissolved in ethyl methyl ketone (5 mL) solvent mixture and left for slow evaporation at room temperature. Single crystals were obtained after 4 days.

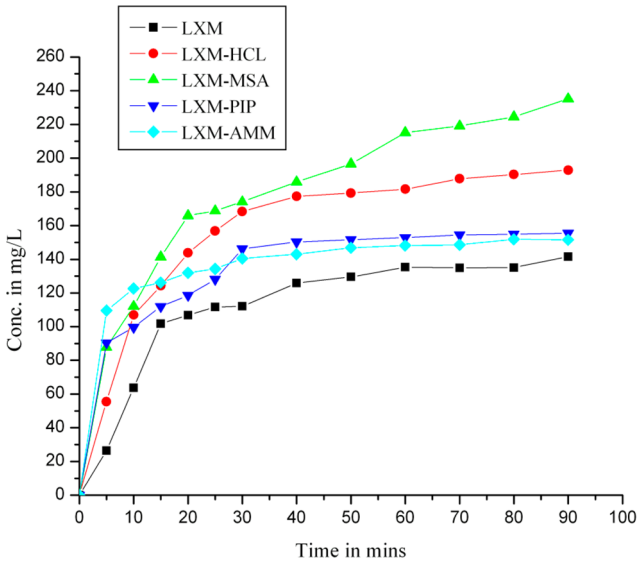

Figure 8. Powder dissolution rates of LXM and its salts in pH 7 phosphate buffer medium.

X-ray Crystallography. X-ray reflections were collected on Oxford CCD X-ray diffractometer (Yarnton, Oxford, UK) equipped with Mo Kα radiation (λ = 0.71073 Å) source. Data reduction was performed using CrysAlisPro 171.33.55 software.[27a] Crystal structures were solved and refined using Olex2-1.0 with anisotropic displacement parameters for non-H atoms.[27b] Hydrogen atoms were experimentally located through the Fourier difference electron density maps in all crystal structures. All O−H, N−H, and C−H atoms were geometrically fixed using HFIX command in SHELX-TL program of Bruker-AXS. A check of the final CIF file using PLATON[28a,b] did not show any missed symmetry. Hydrogen bond distances shown in Table 2 are neutron normalized to fix the D−H distance to its accurate neutron value in the X-ray crystal structures (O−H 0.983 Å, N−H 1.009 Å, and C−H 1.083 Å). X-Seed[28c,d] was used to prepare packing diagrams. Crystallographic.cif files (CCDC Nos. 986789−986793) are available at www.ccdc.cam.ac.uk/data or as part of the Supporting Information.

Powder X-ray Diffraction. Powder X-ray diffraction was recorded on Bruker D8 Advance diffractometer (Bruker-AXS, Karlsruhe, Germany) using Cu Kα X-radiation (λ = 1.5406 Å) at 40 kV and 30 mA power. X-ray diffraction patterns were collected over the 2θ range 5−50° at a scan rate of 1°/min.

Vibrational Spectroscopy. Nicolet 6700 FT-IR spectrometer with a NXR FT-Raman Module was used to record IR spectra of samples dispersed in KBr pellets.

Solid-state NMR Spectroscopy. Solid-state ^{13}C NMR spectra were recorded on Bruker Avance 400 MHz spectrometer (Bruker-Biospin, Karlsruhe, Germany). SS-NMR measurements were carried out on Bruker 4 mm double resonance CP-MAS probe in zirconia rotors with a Kel-F cap at 5.0-kHz spinning rate with a cross-polarization contact time of 2.5 ms and a delay of 8 s. ^{13}C NMR spectra were recorded at 100 MHz and referenced to the methylene carbon of glycine and then recalibrated to the TMS scale ($\delta_{glycine}$ = 43.3 ppm).

Thermal Analysis. DSC was performed on a Mettler Toledo DSC 822e module. Samples were placed in crimped but vented aluminum sample pans. The typical sample size is 4−6 mg, and temperature range was 30−250 °C @ 5 °C/min. Samples were purged by a stream of nitrogen flowing at 150 mL/min. HSM was performed on a PolythermA hot stage and Heiztisch microscope supplied by Wagner & Munz. A Moticam1000 (1.3 MP) camera supported by software Motic Image Plus 2.0 ML was used to record crystal images.

Dissolution and Solubility Measurements. The solubility curves of LXM salts were measured using the Higuchi and Connor method[29] in pH7 phosphate buffer medium at 30 °C. First, the absorbance of a known concentration of the salt was measured at the

dx.doi.org/10.1021/cg500231z | Cryst. Growth Des. 2014, 14, 2945−2953
Ascletis Ex. 2075
Page 7 of 9

Table 5. Powder Dissolution and Solubility of LXM Salts[a]

compound	molar extinction coefficient, ε/ mM cm	equilibrium solubility (mg/L)	solution concentration in mg/L (60 min)	area under the curve, $AUC_{0-60\ min}$ (mg h)/L
LXM	17.28	339.0	100.9	105
LXM−HCl	15.96		143.7 (x1.43)	128 (x1.21)
LXM−MSA	13.08		158.9 (x1.57)	219 (x2.08)
LXM−PIP	16.12	2355.6 (x6.94)	127.1 (x1.26)	109 (x1.03)
LXM−AMM	42.82	879.8 (x2.59)	133.6 (x1.32)	109 (x1.03)

[a]The *n*-fold enhancement compared to LXM is given in parentheses.

given λ_{max} (LXM 374 nm) in pH 7 phosphate buffer medium on Thermo Scientific Evolution 300 UV−vis spectrometer (Thermo Scientific, Waltham, MA). These absorbance values were plotted against several known concentrations to prepare the concentration vs intensity calibration curve. From the slope of the calibration curves, molar extinction coefficients for LXM salts were calculated (The respective molar extinction coefficients (LXM 17.28, LXM-HCL 15.96, LXM-MSA 13.09, LXM-PIP16.12, and LAM-AMM 15.41 mL mg^{-1} cm^{-1} respectively are used to determine the powder dissolution.) An excess amount of the sample was added to 6 mL of pH 7 phosphate buffer medium. The supersaturated solution was stirred at 300 rpm using a magnetic stirrer at 30 °C. After 24 h, the suspension was filtered through Whatman 0.45 μm syringe filter. The filtered aliquots were diluted sufficiently, and the absorbance was measured at the given λ_{max}. The powder dissolution studies of LXM salts was done using 300 mg of LXM, 329 mg of LXM−HCl , 377 mg of LXM−MSA, 369 mg of LXM−PIP, and 313 mg of LXM−AMM (0.8 mmol of each compound), which was directly poured into 500 mL of pH 7 phosphate buffer dissolution medium. The paddle rotation was fixed at 100 rpm, and dissolution experiments were continued up to 90 min at 37 °C. At regular intervals, 5 mL of the dissolution medium was withdrawn and replaced by an equal volume of fresh medium to maintain a constant volume. The AUC was calculated using the linear trapezoidal rule of drug bioavailability.[30] The nature of the solid samples after solubility/dissolution measurements was verified by PXRD to determine if there was any phase transformation.

■ ASSOCIATED CONTENT

Supporting Information

ORTEP plots, IR spectra, DSC heating curves, PXRD patterns, ss-NMR, and crystallographic information files. This material is available free of charge via the Internet at http://pubs.acs.org.

■ AUTHOR INFORMATION

Corresponding Author

*E-mail: ashwini.nangia@gmail.com.

Notes

The authors declare no competing financial interest.

■ REFERENCES

(1) Wermuth, C. G., Stahl, P. H., Eds.; *Handbook of Pharmaceutical Salts. Properties, Selection and Use*, Wiley-VCH: Weinheim, 2002.

(2) Electronic databases, FDA documents; www.fda.gov/cder/guidance (accessed 20 January 2014).

(3) GRAS chemicals list may be accessed at www.fda.gov/Food/FoodIngredientsPackaging/GenerallyRecognizedasSafeGRAS/GRASSubstancesSCOGSDatabase/default.htm (accessed 20 January 2014).

(4) (a) Back, K. R.; Davey, R. J.; Grecu, T.; Hunter, C. A.; Taylor, L. S. *Cryst. Growth Des.* **2012**, *12*, 6110−6117. (b) Sanphui, P.; Goud, N. R.; Khandavilli, U. B. R.; Bhanoth, S.; Nangia, A. *Chem. Commun.* **2011**, *47*, 5013−5015. (c) Nangia, A. *Acc. Chem. Res.* **2008**, *41*, 595−604.

(5) (a) Childs, S. L.; Chyall, L. J.; Dunlap, J. T.; Smolenskaya, V. N.; Stahly, B. C.; Stahly, G. P. *J. Am. Chem. Soc.* **2004**, *126*, 13335−13342. (b) Aakeröy, C. B.; Forbes, S.; Desper, J. *J. Am. Chem. Soc.* **2009**, *131*, 17048−17049. (c) Suresh, K.; Goud, N. R.; Nangia, A. *Chem.—Asian J.* **2013**, *8*, 3032−3041. (d) Yan, Y.; Chen, J. M.; Geng, N.; Lu, T. B. *Cryst. Growth Des.* **2012**, *12*, 2226−2233.

(6) (a) Cherukuvada, S.; Nangia, A. *CrystEngComm* **2011**, *13*, 759−762. (b) Goud, N. R.; Suresh, K.; Sanphui, P.; Nangia, A. *Int. J. Pharm. Sci.* **2012**, *439*, 63−72.

(7) Serajuddin, A. T. M. *J. Pharm. Sci.* **1999**, *88*, 1058−1066.

(8) (a) Yu, L. *Adv. Drug Delivery Rev.* **2001**, *48*, 27−42. (b) Graeser, K. A.; Strachan, C. J.; Patterson, J. E.; Gordon, K. C.; Rades, T. *Cryst. Growth Des.* **2008**, *8*, 128−135.

(9) FDA BCS classification system for guidance. http://www.fda.gov/AboutFDA/CentersOffices/OfficeofMedicalProductsandTobacco/CDER/ucm128219.htm.

(10) (a) Serajuddin, A. T. M. *Adv. Drug Delivery Rev.* **2007**, *54*, 603−616. (b) Goud, N. R.; Suresh, K.; Nangia, A. *Cryst. Growth Des.* **2013**, *13*, 1590−1601. (c) Ong, W.; Cheung, E. Y. K.; Schultz, A.; Smith, C.; Bourassa, J.; Hickey, M. B. *CrystEngComm* **2012**, *14*, 2428−2434. (c) Du, M.; Zhang, Z.; Guo, W.; Fu, X. *Cryst. Growth Des.* **2009**, *9*, 1655−1657. (d) Huang, X.; Zhang, Z.; Zhang, Q.; Wang, L.; He, M.; Chen, Q.; Song, G.; Wei, L.; Wang, F.; Du, M. *CrystEngComm* **2013**, *15*, 6090−6100.

(11) (a) Brunton, L. L., Lazo, J. S., Parker, K. L., Eds.; *Goodman & Gilman's: The Pharmacological Basis of Therapeutics*, 11th ed.; McGraw Hill Medical Publishing, New York, 2006, 700−701. (b) Atzpadien, E.; Mehdi, N.; Clarke, D. *J. Food Anal. Chem. Toxicol.* **1997**, *35*, 465−474. (c) Vane, J. R.; Botting, R. M. *Int. J. Tissue React.* **1998**, *20*, 3−15. (d) Rao, R. N.; Meena, S.; Rao, A. R. *J. Pharm. Biomed. Anal.* **2005**, *39*, 349−363.

(12) Hall, P. E.; Derry, S.; Moore, R. A; McQuary, H. J. *Cochrane Database Syst. Rev.* **2011**, Issue 4, CD007441.

(13) Zhang, J.; Tan, X.; Gao, J.; Fan, W.; Gao, Y.; Qian, S. *J. Pharm. Pharmacol.* **2013**, *65*, 44−52.

(14) (a) Anjankumar, P. B.; Najmuddin, M.; Upendhra, K.; Hariprasanna, R. C. *Int. J. Res. Pharm.* **2011**, *2*, 130−133. (b) Patil, A. L.; Patil, S. S. *Int. J. Pharm. Technol. Res.* **2012**, *4*, 201−207.

(15) Nijhawan, M.; Santhosh, A.; Babu, P. R.; Subrahmanyam, C. V. *Drug Dev. Ind. Pharm.* DOI: 10.3109/03639045.2013.804834.

(16) Nath, N. K.; S. Kumar S, S.; Nangia, A. *Cryst. Growth Des.* **2011**, *11*, 4594−4605.

(17) (a) Patel, J. R.; Carlton, R. A.; Needham, T. E.; Chichester, C. O.; Vogt, F. G. *Int. J. Pharm. Sci.* **2011**, *405*, 142−153. (b) Bolla, G.; Sanphui, P.; Nangia, A. *Cryst. Growth Des.* **2013**, *13*, 1988−2003. (c) Cheney, M. L.; Weyna, D. R.; Shan, N.; Hanna, M.; Wojtas, L.; Zaworotko, M. J. *Cryst. Growth Des.* **2010**, *10*, 4401−4413. (d) Weyna, D. R.; Cheney, M. L.; Shan, N.; Hanna, M.; Zaworotko, M. J.; Sava, V.; Song, S.; Sanchez-Ramos, J. R. *Mol. Pharmaceutics* **2012**, *9*, 2094−2102.

(18) (a) Bernstein, J.; Davis, R. E.; Shimoni, L.; Chang, N. L. *Angew. Chem., Int. Ed. Engl.* **1995**, *34*, 1555. (b) Etter, M. C. *Acc. Chem. Res.* **1990**, *23*, 120. (c) Etter, M. C. *J. Phys. Chem.* **1991**, *95*, 4601.

(19) (a) Rychkov, D.; Boldyreva, V.; Tumanov, N. A. *Acta Crystallogr.* **2013**, *C69*, 1055−1061. (b) Thakuria, R.; Cherukuvada, S.; Nangia, A. *Crystal Growth Design.* **2012**, *12*, 3944−3953. (c) S. Kumar S, S.; Thakuria, R.; Nangia, A. *CrystEngComm* **2014**, DOI: 10.1039/C3CE42324G.

(20) Cruz-Cabeza, A. J. *CrystEngComm* **2012**, *14*, 6362−6365.

Ascletis Ex. 2075
Page 8 of 9

(21) (a) André, V.; Fernandes, A.; Santos, P. P.; Duarte, M. T. *Cryst. Growth Des.* **2011**, *11*, 2325−2334. (b) Karki, S.; Friščić, T.; Fábián, L.; Jones, W. *CrystEngComm* **2010**, *12*, 4038−4041.
(22) Silverstein, R. M. *Spectrometric Identification of Organic Compounds*, 6th ed.; John Wiley & Sons: New York, 2002.
(23) Vogt, F. G.; Clawson, J. S.; Strohmeier, M.; Edwards, A. J.; Pham, T. N.; Watson, S. A. *Cryst. Growth Des.* **2009**, *9*, 921−937.
(24) (a) Stanton, M. K.; Bak, A. *Cryst. Growth Des.* **2008**, *8*, 3856−3862. (b) Bak, A.; Gore, A.; Yanez, E.; Stanton, M.; Tufekcic, S.; Syed, R.; Akrami, A.; Rose, M.; Surapaneni, S.; Bostick, T.; King, A.; Neervannan, S.; Ostovic, D.; Koparkar, A. *J. Pharm. Sci.* **2008**, *97*, 3942−3956.
(25) (a) Takagi, T.; Ramachandran, C.; Bermejo, M.; Yamashita, S.; Yu, X. L.; Amidon, G. L. *Mol. Pharmaceutics* **2006**, *3*, 631−643. (b) Lipinski, C. A.; Borchardt, R. T.; Kerns, E. H.; Thakker, D. R.; Wang, B. In *Pharmaceutical Profiling in Drug Discovery for Lead Selection*; AAPS Press, Arlington, VA, 2004; pp 93−125.
(26) Dressman, J. B.; Amidon, G. L.; Reppas, C.; Shah, V. P. *Pharm. Res.* **1998**, *15*, 11−22.
(27) (a) *CrysAlis CCD and CrysAlis RED*, versions 1.171.33.55; Oxford Diffraction: Oxford, 2008. (b) Dolomanov, O. V.; Bourhis, L. J.; Gildea, R. J.; Howard, J.A. K.; Puschmann, H. *J. Appl. Crystallogr.* **2009**, *42*, 339−341. (c) Berge, S. M.; Bighley, L. D.; Monkhouse, D. C. *J. Pharm. Sci.* **1977**, *66*, 1−19.
(28) (a) Spek, A. L; *PLATONA Multipurpose Crystallographic Tool*; Utrecht University: Utrecht, The Netherlands, 2002. (b) Spek, A. L. *J. Appl. Crystallogr.* **2003**, *36*, 7−13. (c) Barbour, L. J. *Supramol. Chem.* **2001**, *1*, 189−191. (d) Barbour, L. J. *X-Seed, Graphical Interface to SHELX-97 and POV-Ray*; University of Missouri-Columbia, Columbus, MO, 1999.
(29) Higuchi, T.; Connors, K. A. *Adv. Anal. Chem. Instrum.* **1965**, *4*, 117−122.
(30) Viscomi, G. C.; Campana, M.; Barbanti, M.; Grepioni, F.; Polito, M.; Confortini, D.; Rosini, G.; Righi, P.; Cannata, V.; Braga, D. *CrystEngComm* **2008**, *10*, 1074−1081.

Ascletis Ex. 2075
Page 9 of 9